Geophysical Journal International

Geophys. J. Int. (2018) **214,** 315–330
Advance Access publication 2018 April 06
GJI Seismology

doi: 10.1093/gji/ggy139

The crustal structure in the transition zone between the western and eastern Barents Sea

Alexey Shulgin,[1] Rolf Mjelde,[2] Jan Inge Faleide,[1] Tore Høy,[3] Ernst Flueh[4] and Hans Thybo[1,5]

[1] *Centre for Earth Evolution and Dynamics (CEED), University of Oslo, N-0315 Oslo, Norway. E-mail: alexey.shulgin@geo.uio.no*
[2] *Department of Earth Science, University of Bergen, N-5020 Bergen, Norway*
[3] *Norwegian Petroleum Directorate, N-4003 Stavanger, Norway*
[4] *Helmholtz Centre for Ocean Research, D-24148 Kiel, Germany*
[5] *Eurasia Institute of Earth Sciences, Istanbul Technical University, 34469 Istanbul, Turkey*

Accepted 2018 April 5. Received 2018 April 4; in original form 2017 August 16

SUMMARY

We present a crustal-scale seismic profile in the Barents Sea based on new data. Wide-angle seismic data were recorded along a 600 km long profile at 38 ocean bottom seismometer and 52 onshore station locations. The modelling uses the joint refraction/reflection tomography approach where co-located multichannel seismic reflection data constrain the sedimentary structure. Further, forward gravity modelling is based on the seismic model. We also calculate net regional erosion based on the calculated shallow velocity structure.

Our model reveals a complex crustal structure of the Baltic Shield to Barents shelf transition zone, as well as strong structural variability on the shelf itself. We document large volumes of pre-Carboniferous sedimentary strata in the transition zone which reach a total thickness of 10 km. A high-velocity crustal domain found below the Varanger Peninsula likely represents an independent crustal block. Large lower crustal bodies with very high velocity and density below the Varanger Peninsula and the Fedynsky High are interpreted as underplated material that may have fed mafic dykes in the Devonian. We speculate that these lower crustal bodies are linked to the Devonian rifting processes in the East European Craton, or belonging to the integral part of the Timanides, as observed onshore in the Pechora Basin.

Key words: Crustal structure; Continental shelf; Refraction seismology; Seismic modelling.

1 INTRODUCTION

The investigated region coincides with the area separating the Barents shelf into its western and eastern parts with significantly different basin architecture and evolution. Earlier studies of the deep crustal structure have been reported on the Norwegian side (Breivik *et al.* 2003, 2005; Ritzmann & Faleide 2007; Clark *et al.* 2013; Gernigon *et al.* 2014), as well as on the Russian side (Sakoulina *et al.* 2000; Roslov *et al.* 2009; Ivanova *et al.* 2011). Regional 3-D lithospheric models covering the wider Barents–Kara Sea area have also been constructed (Ritzmann *et al.* 2007; Hauser *et al.* 2011; Klitzke *et al.* 2015). The former disputed area between Norwegian and Russian territories has not been studied before, making it difficult to combine existing structural models. Furthermore, the new border line is approximately co-located with the major structural change on the Barents shelf associated with the Caledonian orogeny, complicating the construction of a unified model. The eastern Barents Sea has mainly old Timanian basement overlain by massive sedimentary cover reaching 20 km thickness, while the western Barents Sea developed on top of younger Caledonian basement with much thinner sedimentary deposits. Recently, several multichannel seismic (MCS) acquisition campaigns have been initiated in Norwegian waters prior to industrial licensing and subsequent drilling projects. However, deep seismic profiles are required for understanding of the regional crustal structure. Here we present the results from the first wide-angle seismic profile located within this zone. The seismic profile is located at the transition from the western to eastern parts of the Barents shelf. The interpretation of the crustal structure in this transition may enhance our understanding of complex tectonic evolution of the Greater Barents Sea and link national models on two sides of the border.

2 REGIONAL TECTONIC SETTING AND GEOLOGICAL EVOLUTION

The Barents Sea is a part of the Arctic region, comprising areas of different geological evolution caused by several large-scale tectonic adjustments. The interaction of the Baltica, Laurentian and Siberian plates, together with smaller continental blocks, is the basis for the

formation of the current Barents shelf crust (Marello *et al.* 2013). At present, the overall crustal basement configuration is not well understood. As the area attracts interest due to its petroleum potential, the sedimentary structure has been intensively studied over the last decades. However, the knowledge on the crustal structure is still sparse and scattered due to the existence of a limited number of deep seismic profiles. The current tectonostratigraphic/geodynamic models for the Barents Sea (e.g. Ritzmann & Faleide 2009; Henriksen *et al.* 2011a; Gernigon *et al.* 2014; Gac *et al.* 2016) as well as more recent regional crustal models (Artemieva *et al.* 2006; Ritzmann *et al.* 2007; Barrere *et al.* 2011, Marello *et al.* 2013; Klitzke *et al.* 2015) show the complex structural configuration and the need to expand the number of deep crustal observations to improve the models.

The southern part of the study area (Fig. 1) is located on the Baltic cratonic basement of Meso-Neo Archean age to the south of the transition to the continental shelf. The continental shelf of the Barents Sea is located on an assemblage of terranes, which originate from three major orogenic events in the area: Timanian, Caledonian and Uralian (Fig. 1).

The tectonic history reflected in the present geological settings show a prominent change from east to west. The western Barents Sea is underlain by the Caledonian basement, while the eastern Barents Sea has Timanian basement. The transition area of *ca.* 100 km wide between them is identified from the aeromagnetic data (Fig. 1; Gernigon & Brönner 2012). Offshore, the study area is located to the eastern side of the transition area, suggesting that the underlying basement is of Timanian age. The Timanian orogeny influenced mostly the southeastern corner of the East Barents Sea, including the areas of the present Timan-Pechora Basin. Timan orogeny developed as fold-and-thrust belt along the northeastern margin of Baltica, during the late Neoprotorozoic—early Cambrian (Kostyuchenko *et al.* 2006; Gee *et al.* 2008). The general structural trends of the Timanian orogeny show NW-SE orientation, also in northeast Norway. It is commonly accepted that the southern part of the Barents Sea was also affected, but the NW offshore extent of the Timanian trend is still enigmatic (Olovyanishnikov *et al.* 2000; Roberts & Siedlecka 2002; Pease & Scott 2009). The Trollfjorden-Komagelva Fault Zone is assumed to mark the southern extent of the Timanian terranes in northernmost Norway.

The crustal architecture to the west of the study area is mostly characterized by the strong overprint of the Caledonian event. The Caledonian orogeny caused by the collision of Laurentia and Baltica, which began in the early Ordovician and culminated in the mid Silurian to early Devonian, mostly influenced the western Barents Sea (Roberts 2003; Ritzmann & Faleide 2007; Gee *et al.* 2008; Gernigon & Brönner 2012). The major structural trends associated with the Caledonian orogeny are in the N-S to NE-SW direction (Gudlaugsson *et al.* 1998; Breivik *et al.* 2005; Faleide *et al.* 2008). However, the offshore orientation of the Caledonian structures has been questioned, based on recently collected aeromagnetic data (Gernigon & Brönner 2012). The NE-SW trend, especially in the southwest Barents Sea, appears to reflect later overprint by the Carboniferous rift structures (Faleide *et al.* 2018).

On the Norwegian mainland the basement is an assemblage of two terrane types: the autochthonous rocks of the Baltic Shield (Meso-Neo Archean crystalline complexes) and the Caledonian allochthons, which represent the remnants of a Baltoscandian rifted margin system including shelf successions, oceanic and arc units and exotic rocks with Laurentian affinities (Roberts 2003). In northernmost Norway the Caledonian basement extends into the Barents shelf, but its geometry, orientation and extent are still largely undefined due to the presence of relatively thick layers of younger sedimentary rocks (Ritzmann & Faleide 2007; Faleide *et al.* 2008; Gee *et al.* 2008; Barrere *et al.* 2011). As Caledonian terranes are found on Svalbard (Gee *et al.* 2006), the structural features associated with the Caledonian Deformation Front are located out in the Barents Sea (Fig. 1), but its location is still not fully constrained.

The onshore part in the southern end of the profile (Fig. 1), located on the Baltic craton, has experienced little change at least since the Neo-Archean. The northwestern part of the craton was involved in the Caledonian orogeny, bounded by distinct onshore faults on the western edge of the transition area. To the east, the craton continues on the Kola Peninsula, without any major changes.

The offshore evolution shows a more complex history. The eastern part of the Barents shelf has a crust of Timanian age covered by a very thick sedimentary cover, overlying relatively strong and thick lithosphere (Klitzke *et al.* 2015; Gac *et al.* 2016; Faleide *et al.* 2018). This is contrary to the west, where the basement is Caledonian overlain by a thinner sedimentary cover (with thick Devonian strata) on a weak and somewhat thin lithosphere. The eastern Barents Sea is characterized by a large regional size sag basin, while in the western Barents Sea a platform with numerous rift basins is present. Several rifting episodes associated with the opening of the North Atlantic (Faleide *et al.* 1993; Johansen *et al.* 1994) dominated the evolution of the western Barents Sea in Late Palaeozoic—Mesozoic times. In addition, several magmatic events associated with the High Arctic Large Igneous Province and producing intrusive dykes and sills, occurred in Early Cretaceous (Maher 2001; Corfu *et al.* 2013; Polteau *et al.* 2016). Such magmatic bodies have been identified from seismic data in the eastern Barents Sea (Ivanova *et al.* 2011; Polteau *et al.* 2016; Minakov *et al.* 2017) and offshore Svalbard (Grogan *et al.* 1998; Minakov at al. 2012a). The western Barents shelf is bounded by the present day continental margin (Faleide *et al.* 2008).

The youngest major orogenic event influencing the evolution of the larger Barents Sea area (mostly the eastern part) is the Uralian. The beginning of the event in Early Carboniferous is associated with onset of subduction of the Uralian Ocean under the Siberian craton (Churkin *et al.* 1981). The later collision in Early Permian of the Siberia, Baltica and Laurentia plates is manifested by generation of the Ural mountain chain (Otto & Bailey 1995). The fold-and-thrust belt on Novaya Zelmya may be considered a structural continuation of the Ural Mountains (Puchkov 2002), in spite of its large geometrical offset from the general direction of the Urals (Pease 2011). The geometry of the island is reflected in the major structures of the eastern Barents Sea, and is associated with the Uralian deformation. The final upthrusting of Novaya Zemlya occurred in the Late Triassic—Early Jurassic times (Faleide *et al.* 2018), which is younger than the Polar Urals.

The late Cenozoic uplift affected the entire Barents shelf unevenly (Anell *et al.* 2009; Henriksen *et al.* 2011b; Minakov *et al.* 2012b), and initiated strong erosion, which further complicated the structural architecture of the greater Barents Sea shelf.

3 EXPERIMENT SETUP AND DATA

The experiment was carried out in July–August 2012. The profile is located close to and along the border between Russia and Norway on the Norwegian side (Fig. 2). The data obtained from the onshore and offshore surveys were merged into one database used for the modelling.

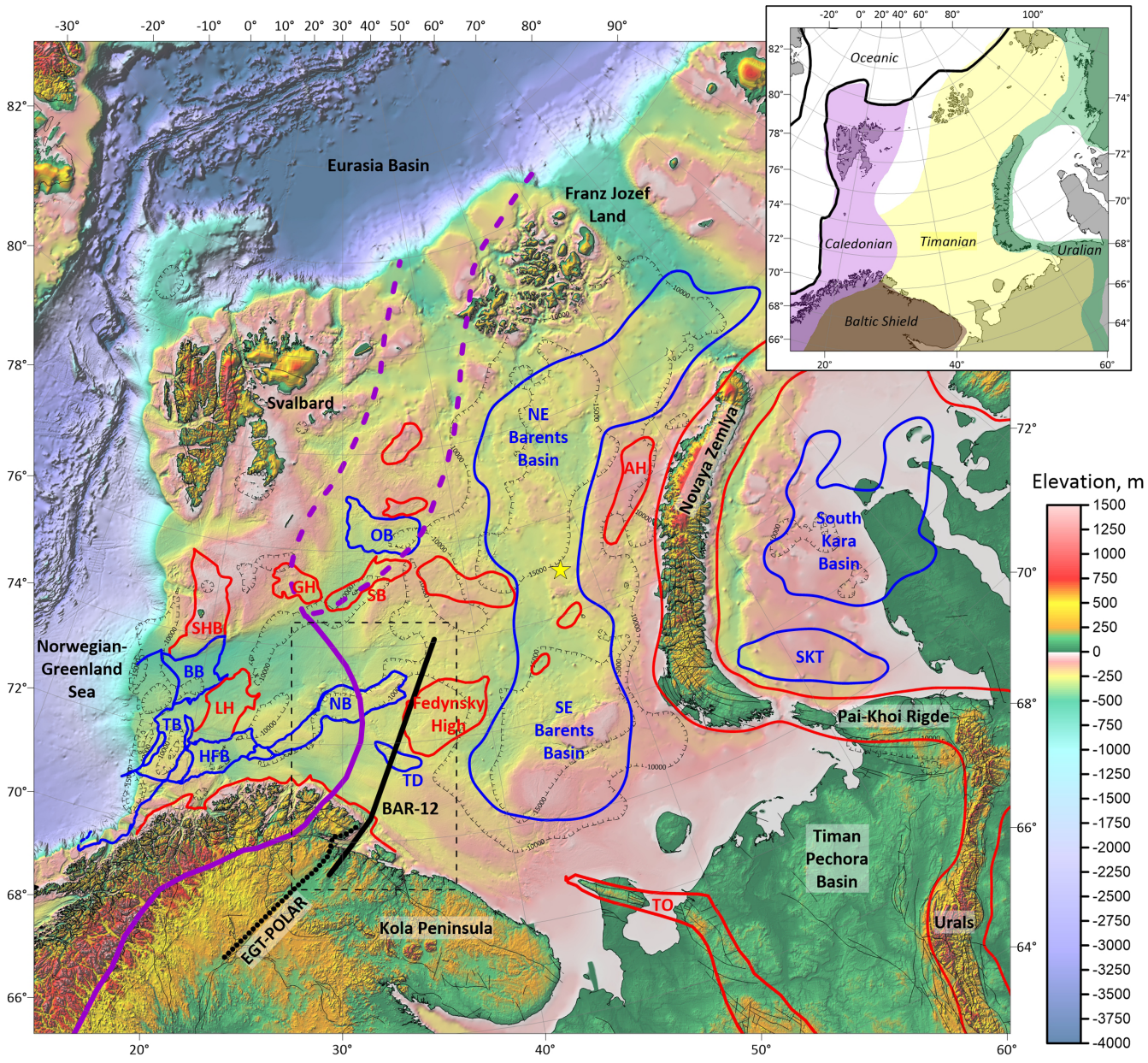

Figure 1. Bathymetric map of the greater Barents Sea, based on the IBCAO data. The major structural highs (red) and lows (blue) are outlined, the contour lines (stippled black) indicate depth to acoustic basement (modified after Klitzke *et al.* 2015): AH—Admiralty High; BB—Bjørnøya Basin; GH—Gardabanken High; HFB—Hammerfest Basin; LH—Lopa High; NB—Nordkapp Basin; OB—Olga Basin; SB—Sørvestsnaget Basin; SKT—South Kara Trough; SHB—Stappen High; TD—Tiddlybanken Basin; TO—Timan Orogen; TB—Troms⊘Basin. The proposed eastern extent of the Caledonian Domain (purple line) is based on the geological data and the analysis of the magnetic data offshore (Gernigon & Brönner 2012). Major onshore faults are shown by thin black lines. Locations of discussed seismic profiles—thick black lines. Star marks the location of the reference drillsite 'Ludlovskaya'. The insert map shows the distribution of the basement domains (modified after Faleide *et al.* 2018). Black dashed box shows the extent of Fig. 2.

3.1 Marine survey

The marine part of the experiment was carried out aboard the Norwegian R/V 'Håkon Mosby'. It included deployment of 20 ocean bottom seismometers (OBS; Bialas & Flueh 1999) for recording of wide-angle seismic data along the profile (Fig. 2). Data acquisition was carried out on two independent subprofiles. On the first subprofile, 20 OBSs were deployed (OBS numbers: 1–20) from the Varanger Fjord northwards towards the Tiddlybanken Basin. For the northern subprofile, 18 OBSs were deployed (OBS numbers: 21–38), from the Tiddlybanken Basin to the northern end of the profile around the Nordkapp Basin (Fig. 2). Two instruments (19 and 20) stayed on the sea bottom during the entire experiment, and recorded air-gun shots from both profiles. This was done to ensure sufficient overlap of the refracted rays along the two subprofiles. All deployed OBSs worked correctly, except at location OBS-6, where no data could be retrieved from the instrument. The resulting composite marine profile is 515 km long with an average distance between OBSs of 13.5 km.

All OBSs were instrumented with a hydrophone and a three-component seismometer. In general, the signal-to-noise ratio is best

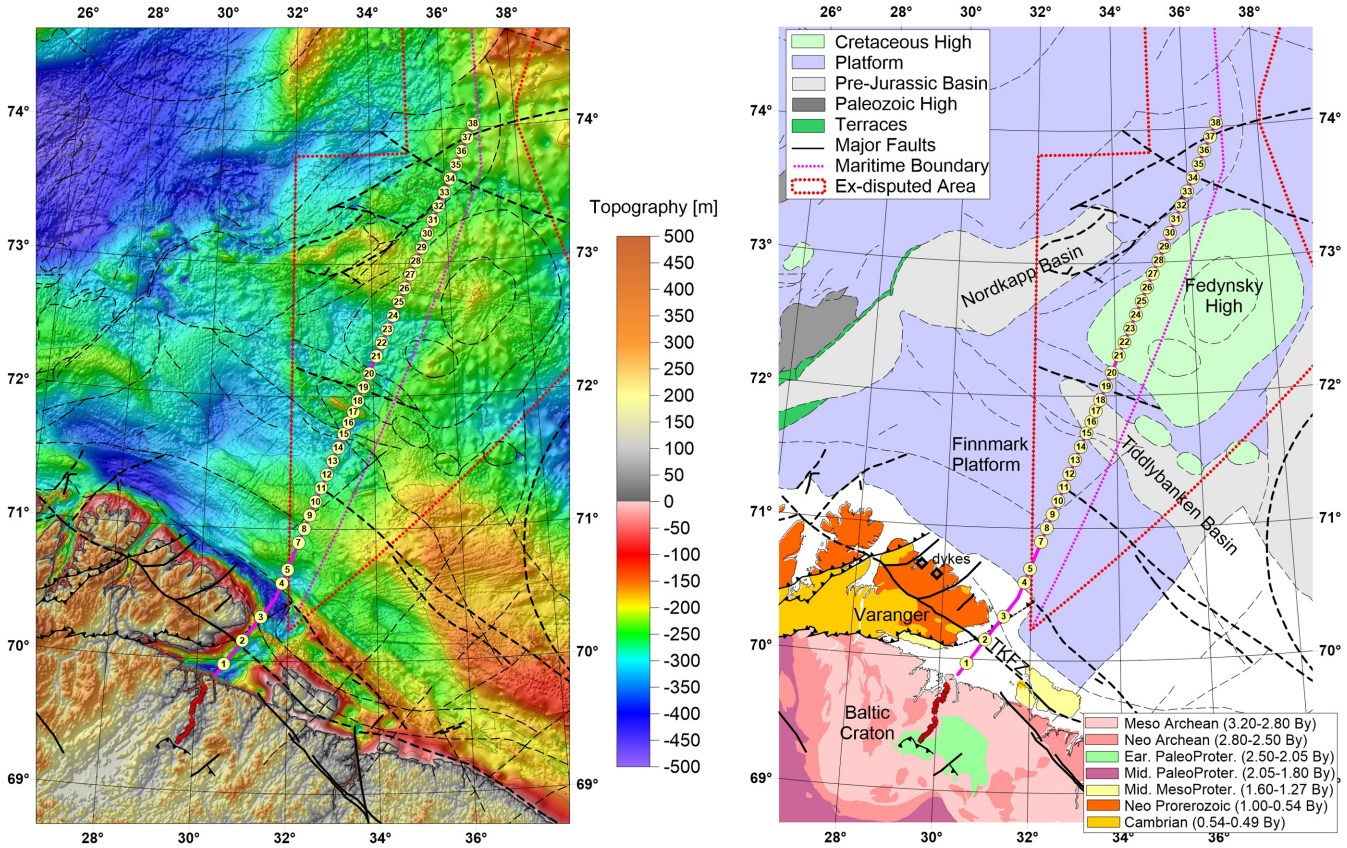

Figure 2. Study area. The left panel shows the combined topography/bathymetry map in the south-central Barents Sea. The right panel is a simplified tectono/geological map, modified after Gabrielsen *et al.* (1990); the land geology is after USGS Arctic Geology Map. The location of the profile and ocean bottom/land seismometers are marked on both panels. TKFZ—Trollfjorden-Komagelva Fault Zone.

on the hydrophone records, but the recordings on the vertical seismometer were also used when possible.

The seismic source included 4 Bolt air guns with a total volume of 4800 inch^3, being fired at 135–138 bar. The shooting interval was 200 m, GPS controlled. For each marine subprofile the shooting was extended about 70 km beyond the last OBS position, thus providing a total data overlap between the profiles of about 100 km. At the northern end of the profile shooting was terminated at the maritime border. Parts of the southern subprofile were shot twice due to technical problems.

Processing of the OBS data (see Supporting Information Fig. S1 for the main processing flow) included localization of the OBS on the ocean floor using the direct arriving water-wave to correct for possible drift during instrument descend. Time-gated predictive deconvolution was applied to remove the air bubble reverberations and thereby improving the signal-to-noise ratio. Finally, a time and offset variant Butterworth filter, where the band-pass changes from 0.8–7.5–65–86 Hz at near offsets towards lower frequencies (0.8–4.5–20–30 Hz) at far offset and late record times, was applied to correct for frequency changes caused by signal attenuation. Bandpass changes are discrete in four windows, which are linearly ramped over 1 s traveltime.

3.2 Onshore survey

In order to resolve the crustal structure below the Varanger Peninsula and the Archean part of the craton, the marine profile was extended onshore toward the south. Along the continuation of the marine part, 52 seismic land stations were deployed (Fig. 2) with an average spacing of 1 km, resulting in a 70 km inland extension of the profile. The land stations were equipped with a single-channel vertical geophone and deployed along available roads. The instruments were deployed in 0.5–1 m deep pits, at least 10 m from the road (where possible). The stations recorded the air-gun shots from the southern marine subprofile. Due to logistical difficulties the shots from the northern line were not recorded. The processing of the land data was mostly limited to band-pass filtering and gain corrections. The overall data quality ranges from excellent to poor, due to the noise problems at some locations (heavy traffic, quarry in the proximity). Out of 52 deployed stations 35 recorded data with reasonable signal-to-noise level and these were used for the modelling.

3.3 Data examples

Example seismic sections are shown in Fig. 3. For the major part of the instruments clear first arriving phases (Pg and Pn) are observed for offsets reaching 200–210 km from the stations. Reflection phases are identified in the records, including reflections from the basement, middle and lower crust, and Moho (PmP), as well as multiple reflections from these interfaces. As information from the co-located MCS line is available, the reflections within the sedimentary units recorded by the OBSs are beyond scope for this study. For the shallow portion of the model, the data from the MCS line is used to constrain the sedimentary sequences for the modelling of the crustal structure.

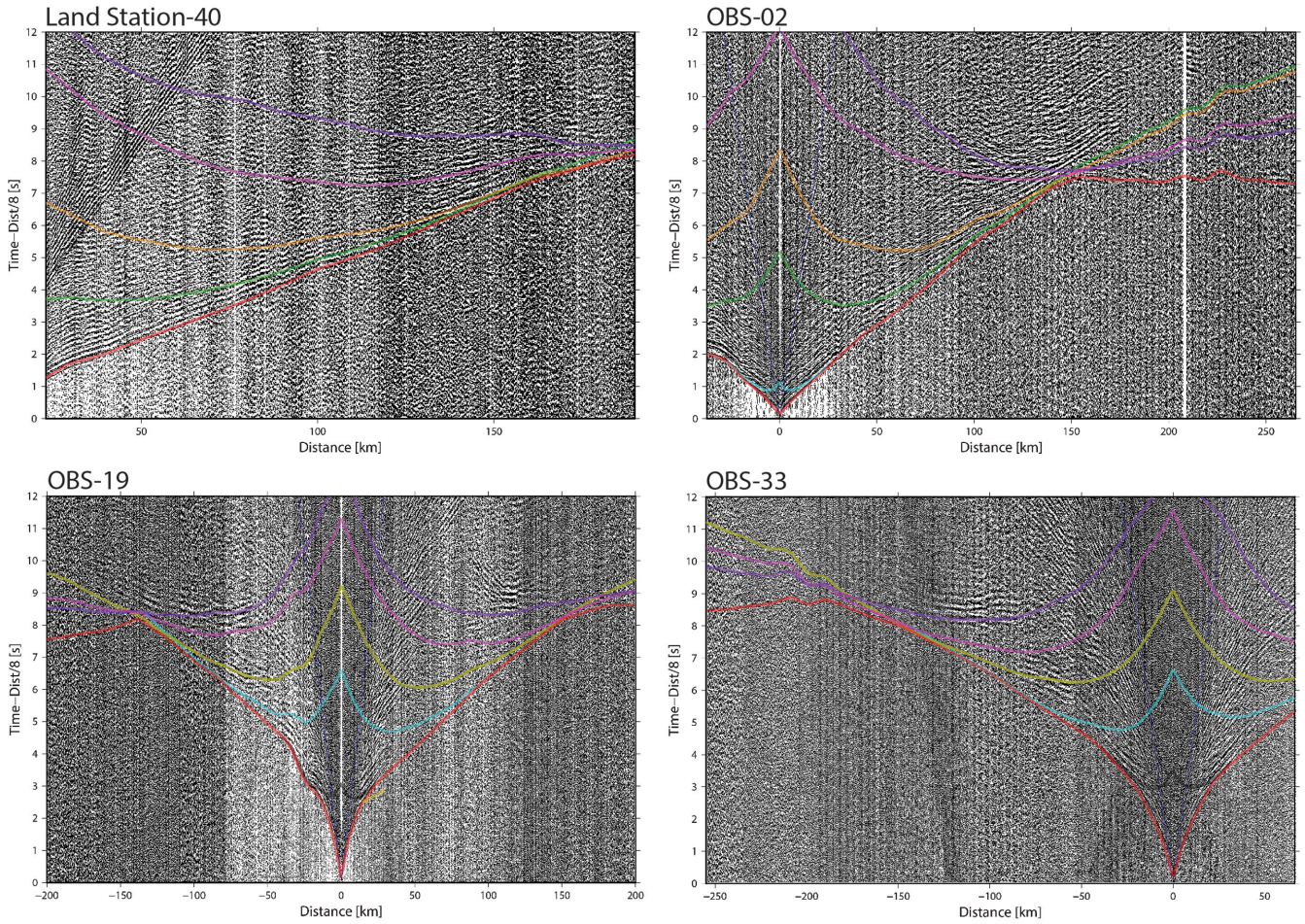

Figure 3. Examples of the seismic data sections from OBS and land stations (see Fig. 2 for locations). The coloured lines show the predicted traveltimes computed from the final Vp tomography model. Red—refracted first arrivals (Pg and Pn). Black—reflection from the base Carboniferous sedimentary strata. Blue—reflection from the crystalline basement. Green—reflection from upper/middle crust boundary. Yellow—reflection from the top of the lower crust. Magenta—reflection from the bottom of the lower crust. Violet—reflection from the Moho (PmP).

4 MODELLING

The final data set used for the crustal modelling includes wide-angle seismic records from 37 OBSs and 35 land locations. In addition, information on the sedimentary structure offshore is available from the co-located MCS profile (Fig. 4a). Furthermore, gravity data were collected onboard the vessel during the cruise. The modelling procedure includes the use of all these data in order to constrain a velocity and density model along the profile (Supporting Information Fig. S1).

4.1 MCS data

The industrial quality MCS data interpretation was available in the early stage of the project (Fig. 4a). The detailed sedimentary structure obtained from this profile is incorporated into the starting velocity model for the tomographic inversion of the refracted/reflected traveltimes. The MCS model includes the geometry of numerous sedimentary strata ranging from early Cretaceous to early-mid Carboniferous in age. For the area below the Finnmark Platform the geometry of the acoustic basement is also retrieved. Due to propriety agreement, the detailed velocity profiles obtained from the velocity analysis of MCS data are not available. In order to constrain the starting model in the depth domain, constant velocities are assigned for each layer and later recalculated from two-way-traveltimes (TWTs) based on the known TWT to the reflectors.

4.2 Forward modelling

Prior to tomographic inversion, forward seismic ray-tracing modelling is carried out. The main goal of this step is to properly identify the main reflection and refraction phases from the seismic sections, as well as to incorporate the MCS model into the starting model for the tomographic inversion. The modelling is carried out with the SeisWide software (*http://seismic.ocean.dal.ca/~seismic/utilities/seiswide/index.php*), which is a Windows platform GUI built on the original RayInvr package (Zelt & Smith 1992). Based on the forward modelling the reflections from the acoustic basement, middle crust, lower crust, and Moho are successfully identified for all OBS and land stations. This allows the construction of a consistent refraction/reflection traveltime database for all available sources and receivers for the seismic tomography approach. The final seismic data set for the inversion consists of *ca.* 35 000 refracted and *ca.* 45 000 reflected traveltimes for the observed phases.

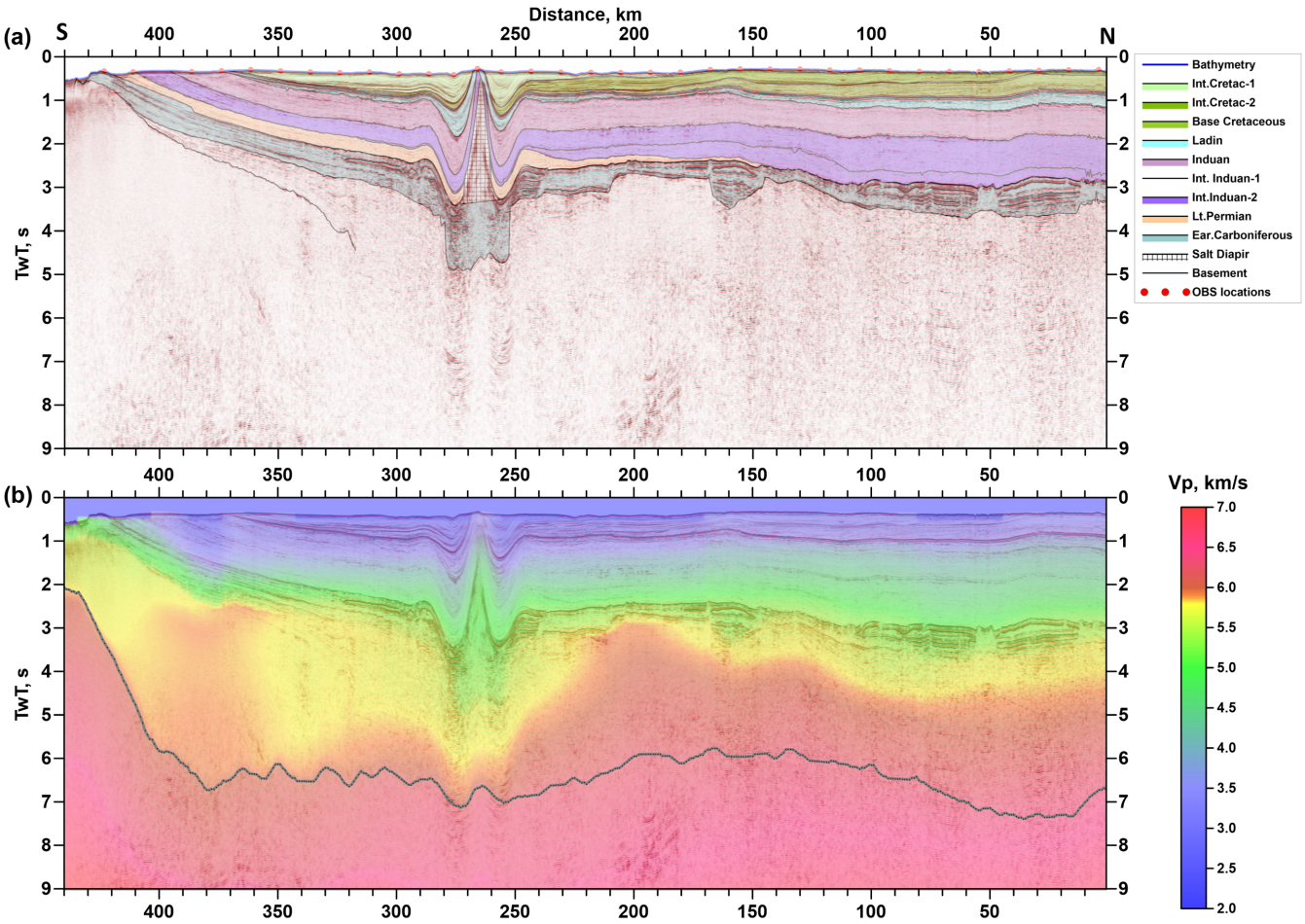

Figure 4. (a) Line-drawing interpretation of the co-located MCS profile by the NPD. The major sedimentary units are identified and used for construction of the starting model for the tomographic inversion. (b) Combined plot of MCS and wide-angle seismic interpretations. The final tomography model is superimposed on the MCS data after conversion from depth to two-way-traveltime. The background colour shows the Vp velocity obtained in the tomographic inversion (colour scale is modified to emphasise the basement). Grey lines—reflector geometry in time domain.

4.3 Tomography inversion

The seismic tomography inversion is carried out with the 2-D joint reflection/refraction code—Tomo2D (Korenaga *et al.* 2000). The starting model is based on the MCS model for the sedimentary cover and the results from the forward modelling of the crystalline crust. The inversion is done according to a 'top to bottom' approach. The overall model is built by recovering the velocity structure and the geometry of the individual layer from the surface and progressively downwards. The focus of the modelling is to obtain the velocity structure of the crystalline crust, assuming that the sedimentary sequences are adequately described in detail by interpretation of the MCS profile. In addition, the structure of the subcarbonate platform sedimentary strata is considered by our modelling procedure, as it is not resolved in the seismic reflection data.

The tomography model is defined on an irregular 2-D grid. The horizontal spacing is fixed to 500 m, and the vertical spacing is increasing with depth: from 50 m at the surface to 330 m at 60 km depth. Such vertical spacing provides the optimum compromise between vertical resolution and computational time. The geometry of each of the reflectors is computed on a similar horizontal grid at a 500 m interval. The data set of the picked traveltimes consists of about 35 000 refracted and 45 000 reflected arrivals. The pick uncertainties for the refracted arrivals range between 25–60 ms, and 40–100 ms for the reflections. The preferred final tomography model is shown in Fig. 5(a).

The obtained final tomography model is further validated against the MCS data. The Vp tomography model is converted from depth to TWT domain. Fig. 4(b) shows the composite model of the velocity and reflectivity along the profile down to 9 s TWT, approximately corresponding to 25 km depth.

4.4 Gravity validation of seismic model

We test the consistency of the seismic velocity model with gravity data by forward 2-D gravity calculation. A detailed analysis of the density structure is outside the scope of this study, but the gravity results presented provide an independent check on the robustness of the seismic model.

The gravity measurements are based on the ship-borne gravimeter data collected along the profile. The onshore part is not considered in the gravity analysis due to limited data availability and strong 3-D effects, which are difficult to take into account.

The density model is calculated from the final seismic velocity model, using empirical velocity-density conversion relationships for sediments and crystalline crust (Carlson & Herrick 1990; Christensen & Mooney 1995). The model space extends down to 80 km

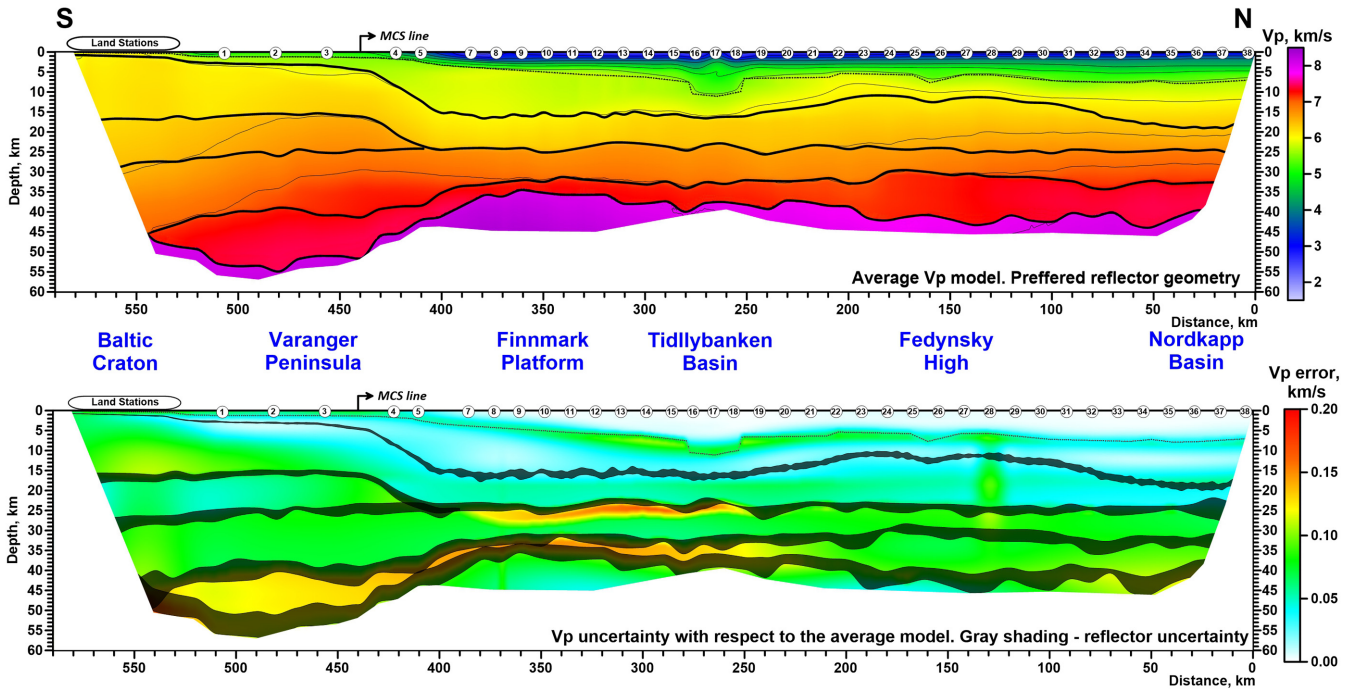

Figure 5. Final Vp model of the profile from the tomographic inversion and the result of the Monte Carlo tests. Top panel: averaged Vp velocity field, thick grey lines—preferred geometry of the crustal reflectors. Bottom panel: standard deviation of the velocity estimation with respect to the averaged value. Grey shading shows the standard deviation of the reflector depth estimation. The Monte Carlo test was performed using 150 semi-random starting models and initial reflectors.

to accommodate potential density variations below the base of the crust, as indicated by the velocity model. For the mantle with Vp $>$ 8.2 km s^{-1} a fixed density value of 3.35 g cm^{-3} was assigned. The velocity-density converted model shows good fit to the regional gravity data (Fig. 6), suggesting that the velocity model and the overall geometry of the crustal layers is correctly described.

4.5 Monte Carlo analysis—uncertainties

The assessment of the uncertainties of the tomographic model is addressed by the results of a series of Monte Carlo tests. The final velocity model is taken as a starting point for the tests (RMS of the final model is 86 ms). The upper part of the model consisting of the sedimentary sequences is considered well constrained from the independent MCS data, and is therefore not part of the analysis, and the model uncertainties are only estimated for the depths below early Carboniferous sedimentary strata.

In order to check the uncertainties of the Vp and reflector geometries, Monte Carlo tests are run for each layer individually. Each test includes 25 tomographic inversions with semi-random starting parameters. For each individual inversion the velocities in the starting model are randomly perturbed by $\pm$ 10 per cent with random spatial patterns. Similarly, the starting geometry of each reflector is randomly shifted vertically at each horizontal node within $\pm$ 15 per cent of the depth range. In addition, for each run the individual traveltime are modified by adding a random positive or negative delay within the pick uncertainty error. The results of such 25 tomographic inversions for each layer are statistically analysed to produce the average model/reflector and the standard deviation. The uncertainty analysis includes six layers, resulting in 150 semi-random tomographic inversions. The analysed uncertainties of the final velocity model are shown in Fig. 5(b).

Overall, the model space is resolved within the 0.10–0.15 km s^{-1} range for Vp. The uncertainties of the reflector geometries vary with depth, ranging from $\pm$ 1 km for the acoustic basement to $\pm$ 3 km for the Moho. An important issue is the resolvability of the lowermost crust (Vp $>$ 7.25 km s^{-1}), because high Vp in this layer indicates the presence of high velocity lower crustal bodies (LCBs). Based on the Monte Carlo tests, such bodies are clearly resolved along most of the profiles, including the edges of the profile (50–220 km and 400–540 km), spatially corresponding to the locations of Fedynsky High and Varanger block. However, in the central part of the profile (220–400 km), the presence of a high-velocity layer is unlikely, although the uncertainty is larger in this part.

5 RESULTS

The following results are based on the joint interpretation of the seismic refraction/reflection and gravity data along the new seismic profile (Figs 1 and 2).

5.1 Craton

The southern part of the profile is located inside the Baltic Shield (540–600 km profile distance), bounded by the Trollfjorden-Komagelva Fault Zone to the north. The crustal structure of the craton shows a three-layer division (Fig. 7). The upper crust has a thickness of about 15–16 km, with Vp increasing from 6.0 km s^{-1} at the top to 6.2 km s^{-1} at the bottom. The middle crust with an average thickness of about 10 km is modelled with velocities ranging from 6.3 to 6.4 km s^{-1}. The lower crust with velocities in the range from 6.6 to 6.9–7.0 km s^{-1} has a thickness of 10–15 km. As this area is located close to the edge of the profile, the ray coverage with depth is limited. This prevents detailed study of the Moho geometry

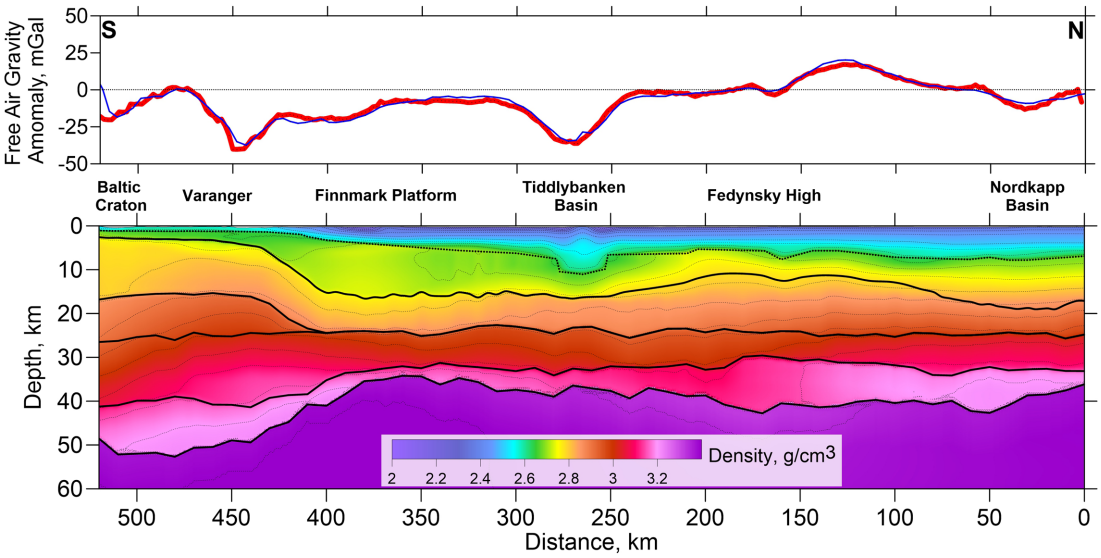

Figure 6. Result of the gravity modelling. The top panel shows the observed (red) and predicted (blue) curves for the Free-Air gravity anomaly along the profile. The bottom panel shows the density model obtained from the Vp tomography results and gravity modelling. Grey lines show the major interfaces identified from the seismic modelling.

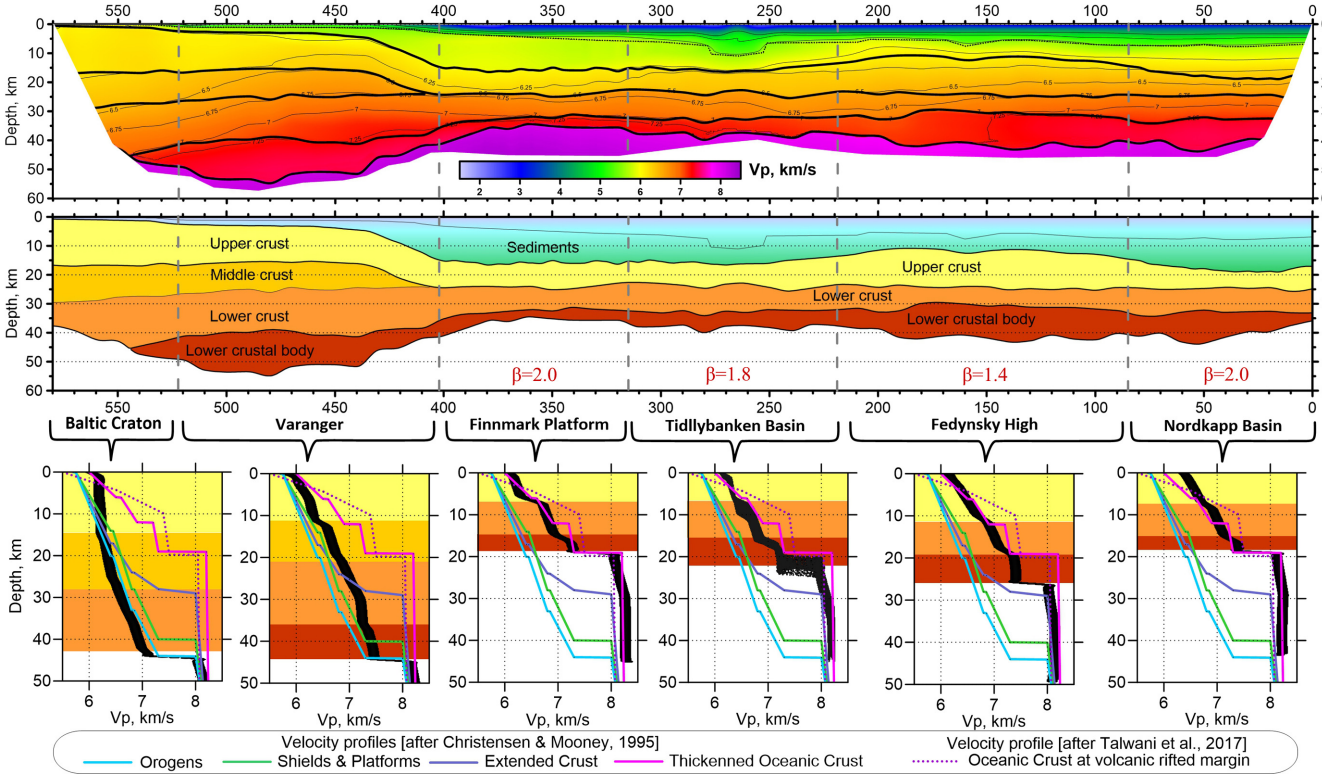

Figure 7. Distribution of Vp with depth along the profile can be separated into six domains, associated with structural changes (approximate domain boundaries are shown by grey stippled lines). Top panel: tomography model; middle panel: simplified structural interpretation. The estimated extension factor is shown in red in the bottom. Six graphs at the bottom show characteristic velocity profiles with depth (black shading) from the top of the basement for each domain. From left (south) to right (north): (1) Baltic craton, (2) Varanger block, (3) Finnmark Platform, (4) Tiddlybanken Basin, (5) Fedynsky High, and (6) Nordkapp Basin. For each domain, characteristic crustal structure is shown by colour-coding as on middle panel. The Vp curves for different tectonic settings (Christensen & Mooney 1995) and (Talwani *et al.* 2017) are plotted for reference.

below the craton. However, based on our estimates the Moho at the northern edge of the Baltic Shield is located at 43–45 km depth.

5.2 Varanger Peninsula terrane

The Varanger terrane (420–540 km distance) is bounded by the Trollfjorden-Komagelva Fault Zone in the south (at shallow depth) and continues for *ca.* 100 km to the north (Herrevold *et al.* 2009;

Fig. 2). The surface expression of the northern limit of the block can be placed at the sharp change in the bathymetry (around 410 km distance) north of the Varanger Peninsula. The northern boundary of the block is most likely dipping towards north, whereas the southern boundary may be dipping southwards, although it is not constrained.

The velocities right below the sea bottom are as high as 5.5 km s^{-1}, increasing to about 5.7 km s^{-1} at 3 km depth, where a reflector is observed. The origin of this boundary is not very clear, but comparison with MCS results from Roberts *et al.* (2011) suggests that this interface may be the contact between Baltic craton basement and the Neoproterozoic metasediments of the Varanger block.

The upper crust has a thickness of 12 km with velocities ranging from 6.0 to 6.3 km s^{-1} at the bottom similar to the cratonic part. The middle crust is characterized by higher Vp than the Baltic Shield, with values ranging from 6.5 to 6.7 km s^{-1}. The thickness of the middle crust is rather uniform around 10 km. At the northern edge of the Varanger block (about 420 km distance), the typical middle crust disappears over 15–20 km horizontal distance.

The lower crust of the block shows high Vp values starting from 6.8 km s^{-1} at the top and reaching 7.2 km s^{-1} at the bottom. Such high velocities are in sharp contrast to the structure of the lower crust of the cratonic domain. In addition to high velocities in the lower crust, we observe a 5–10 km thick layer with even higher velocities forming the lowermost crust. The Vp in this zone is ranging from 7.20 to 7.45 km s^{-1}. The associated gravity modelling suggests densities for this layer to be around 3.1–3.2 g cm^{-3}. The Moho is interpreted to be at a depth of 47–51 km below the Varanger block. Unfortunately, due to limited number of Pn phases, the velocity structure of the uppermost mantle is poorly constrained here.

5.3 Transition zone—Finnmark Platform

The area of the Finnmark Platform (300–420 km distance) is bounded by the Varanger block in the south and extends to the Tiddlybanken Basin in the north (Fig. 2). The MCS data is resolving north dipping sedimentary units which are truncated at the sea bottom. The Devonian molasses deposited in front of the Caledonian mountains in general represent the deepest sedimentary fill (Faleide *et al.* 2018). The MCS data is resolved down to the early Carboniferous and shows evidence for additional older sedimentary deposits below, but the thickness of sedimentary strata (located below carbonate platform and having pre mid-Carboniferous age) and older clastic sedimentary rocks is unresolvable from the MCS data. Based on the tomography results the layer of pre-Carboniferous sedimentary rocks is estimated to be upto 12 km thick with velocities around 5.6–5.8 km s^{-1}. The basement is steeply dipping northward at the proximity of the Varanger block (probably representing a tilted boundary of the block as indicated by the sedimentary structure), and is semi-flat at 15 km depth from around km 390. The upper crust with a thickness of 6–8 km has velocities in the range of 6.0–6.3 km s^{-1}. The lower crust is 7–10 km thick with a Vp of 6.7 km s^{-1} at the top and 6.9–7.0 km s^{-1} at the bottom. The Moho depth is modelled to be 33–35 km. Based on the uncertainty analysis the presence of a very thin layer of high-velocity lowermost crust in the area is possible.

5.4 Tiddlybanken Basin

The Tiddlybanken Basin is located on the northern flank of the Finnmark Platform (220–300 km distance) and is bounded by the fault system adjacent to the Fedynsky High to the north (Fig. 2). The orientation of the basin is NW–SE, parallel to the trace of Trollfjorden-Komagelva Fault Zone, and almost perpendicular to the main rift structures observed in the western Barents Sea (e.g. Nordkapp Basin). The seismic profile is perpendicular to the strike of the basin. The basin structure is identified from the seismic data as a graben structure filled with Carboniferous and younger sediments. It is known that the basin includes salt diapirs. The basin width along the profile is 75–85 km. The salt diapir crossed by the profile at *ca.* km 270 originates from a depth of about 5 km, and based on the stratigraphy the diapirism was active during the Triassic culminating in Cretaceous. However, the salt itself was deposited in the Upper Carboniferous—lowermost Permian. Based on the tomography results there is an additional layer of 6–7 km of pre-Carboniferous sedimentary rocks above the basement in the Tiddlybanken Basin. Most likely, it consists of early Palaeozoic meta-sediments observed above the acoustic basement and a layer of the Devonian sediments which represents molasse deposits from the Caledonian erosion, similar to on the Finnmark Platform.

The crystalline crustal structure below Tiddlybanken Basin is similar to the crust of Finnmark Platform. The upper crust has a thickness of 6–7 km, and is characterized by velocities of 6.2–6.4 km s^{-1}. No significant undulations of the basement or mid-crustal interface are observed in this area. An 8–10 km thick layer with velocities between 6.6 and 6.9 km s^{-1} represents the lower crust. There are indications of a thin 7.3 km s^{-1} layer of lowermost crust below the basin, with thickness most likely not exceeding 1–2 km.

5.5 Fedynsky High

The area north of Tiddlybanken Basin is known as the Fedynsky High (90–220 km distance), and is observed as an elevated area in the bathymetry and gravity data (Fig. 2). The MCS data shows a simple layered sedimentary sequence down to Carboniferous. The Carboniferous-Devonian contact is located at a depth of *ca.* 5 km and shows a complex structure. The presence of a high-velocity carbonate platform is known in the area. The observed seismic velocities in the tomography model, corresponding to the carbonate platform, are around 5.9–6.0 km s^{-1}. High velocities, within the range of 6.0–6.2 km s^{-1} are found above the acoustic basement. It is likely that due to limited resolution, vertical smearing of high velocities in the carbonates is responsible for the increased velocity values for the pre-Carboniferous sedimentary strata. An alternative option is that the acoustic basement is located close to the sea surface, but poorly recovered due to low impedance contrast.

Three distinct crustal layers describe the structure of the crystalline crust below the Fedynsky High. The upper crust has a thickness in the range 8–13 km with velocities of 6.1–6.2 km s^{-1} at the top and increasing to 6.5–6.6 km s^{-1} at the bottom. These values are higher than the upper crust on adjacent segments of the profile, suggesting difference in composition or possibly, high-velocity intrusive bodies within the crustal volume. The velocity structure of the lower crust is within the 6.7–7.0 km s^{-1} range and the thickness of the lower crust is around 6–8 km.

Below the Fedynsky High a large volume of high velocity material is observed in the lowermost crust. This LCB is estimated to have a thickness up to 10 km with a Vp around 7.2–7.3 km s^{-1}. The presence of this volume, as well as the increased velocities in the lower crust and possible uplift of the basement, reflect a complex evolution of the Fedynsky High.

5.6 Nordkapp Basin trend

The northern end of the profile is located on the eastern continuation of the Nordkapp Basin (0–90 km distance; Fig. 2). Along the profile the only manifestation of the basin is a slight increase in thickness of the sedimentary package. The depth to Carboniferous strata (as identified in the MCS data) is around 6 km, but the velocity model indicates an additional 10–11 km thick layer of pre-carbonate platform sedimentary strata of unclear origin. These sediments could also represent molasse deposits originating from the Caledonian erosion and potential older underlying meta-sediments.

The crystalline crustal structure is represented by an upper crust about 7–9 km thick, and a lower crust about 8 km thick. The velocities in the upper crust range from 6.3 to 6.65 km s^{-1}, which are slightly higher than in the cratonic and platform regions, and comparable to the Fedynsky High. The lower crust has Vp in the range 6.9–7.1 km s^{-1}. Such high values are comparable to the lower crust below the Varanger block, whereas the lower crustal Vp is on average lower in all other regions. The geometry of the lowermost crust observed below this portion of the profile is not fully resolved due to the location close to the end of the profile, causing limited depth coverage. However, the Monte Carlo analysis indicates the presence of an 8–10 km thick high velocity lowermost crustal layer (Vp ∼7.3 km s^{-1}) on the southern flank of the basin, probably thinning towards the north.

5.7 Shallow structure along the profile

The co-located multichannel reflection seismic profile (Fig. 4) shows complex evolution of the sedimentary cover, including episodes of strong uplift, tilting and erosion. The southern part of the profile just northeast of the Varanger Peninsula documents a sea bottom exposed stratigraphic sequence from lower Carboniferous at the Varanger–Finnmark Platform transition to Cretaceous towards the Tiddlybanken Basin. The geometry of the sedimentary packages suggests strong uplift and tilting of the Varanger block, accompanied by surface erosion, which is consistent with earlier estimates (Medvedev & Hartz 2015).

The Tiddlybanken Basin is expressed in the sedimentary sequence as a well-resolved graben structure down to early Carboniferous strata, but due to lower resolution in the wide-angle modelling it is difficult to estimate how the pre-Carboniferous sedimentary layers were affected by the graben formation. The salt diapirs present in the basin extend from uppermost Carboniferous—lowermost Permian strata penetrating younger sediments. Based on the thicknesses of the sedimentary layers in the graben zone, the basin formation presumably initiated in early Carboniferous and was later reactivated in both the Triassic and the Cretaceous.

The sedimentary layering on the Fedynsky High indicates a complex uplift history. As the pre-Carboniferous strata are not resolved, it is difficult to estimate the early history. However, the complex geometry of the early Carboniferous strata, including faulting and graben formation, suggests that the initial stage of the uplift started in early Carboniferous. This uplift influenced only the local area around the Fedynsky High, whereas areas further north were not affected. The decreasing thickness of Permian sediments from the Tiddlybanken Basin towards the Nordkapp Basin, including the Fedynsky High, suggests that the second stage of uplift began around the late Permian–Early Triassic and affected the entire northern section of the study area. For the major part of the Mesozoic this area was semi-stable. The later stages of the uplift began around the Late Cretaceous and continued through the Cenozoic.

5.8 Analysis of shallow velocity–depth profiles for uplift and erosion

Estimates of the regional uplift can be obtained from the modelled shallow velocity gradients. Data from the Ludlovskaya borehole site (Fig. 1) can be used as reference. The velocity–depth profile has been reported at this site by Gramberg *et al.* (1985) together with the net erosion estimate of about 750 m. The main assumptions in the estimation of the net erosion rates are: (1) there are no significant compositional variations of the sediments in the upper 2 km; (2) after consolidation of the clastic sediments at maximum burial, resulting in the velocity increase, the velocities are 'frozen' and do not change during uplift. Based on these assumptions, comparison of velocity gradients in the upper 1.5–2 km of the profile allows estimation of net erosion rates with respect to the reference location.

The velocity gradients in the upper 2 km below the sea bottom were extracted from the tomography model with the spatial increment of 1 km (Fig. 8a). The velocity curves are very similar along the profile and their slope is similar to the velocity profile at the reference site in the depth range from 200 to 1100 m. However, the vertical shift of the velocity curves is significant. The precise analysis of the velocity profiles in the slope–vertical-shift domain ($V = \text{slope} \cdot Z + \text{vert.shift}$) (Fig. 8b) shows a linear trend. The slopes for the major part of the profile (except the northern part, around the Nordkapp basin) are similar and around 0.85–0.95 s^{-1}. Since the slopes are semi-constant along the profile, we can estimate the vertical shift, that is, net vertical erosion (Fig. 8c).

Our estimates show a regional uplift and net erosion along the profile ranging from *ca.* 500 to 1500 m. The smallest net erosion rates are estimated in the southern end of the profile on the Finnmark Platform, which is consistent with the observed tilting of the sedimentary strata in the MCS data. The presence of the stable cratonic crust may play a stabilizing role in the vertical motions of adjacent areas. The net erosion rates are monotonically increasing towards the northern end of the profile around the Nordkapp Basin trend. Our estimates are in good correlation with previous results (e.g. Henriksen *et al.* 2011b; Baig *et al.* 2016).

6 DISCUSSION

6.1 Crustal thickness of the cratonic part of the Baltic Shield

Comparison of the obtained model for the Baltic Shield with an earlier crustal model in the area (EGT Polar profile, Fig. 9; Luosto *et al.* 1989) shows good fit between the two interpretations. The two profiles coincide at the onshore part of our profile, whereas the Polar profile extends onshore on the Varanger Peninsula where we deployed OBS stations slightly further east at sea just off the coast. The crustal structure is very similar in the two profiles, although the Polar profile may have better control of the internal boundaries due to better sampling at the southern end of our profile. There is a match in crustal velocities and depths to boundaries and Moho between the profiles. Despite having no shot point at the end of the profile at the north coast of the Varanger Peninsula, the Polar profile also identifies the high velocity in the lowermost crust, although with larger uncertainty than here. The Polar profile also identifies the southward extent of this high-velocity lowermost crustal body at the same location as our profile, which is at the southernmost edge of the part constrained in our profile.

Both models show a trend in the Moho deepening towards the northern edge of the craton. As the thickness of the upper and middle

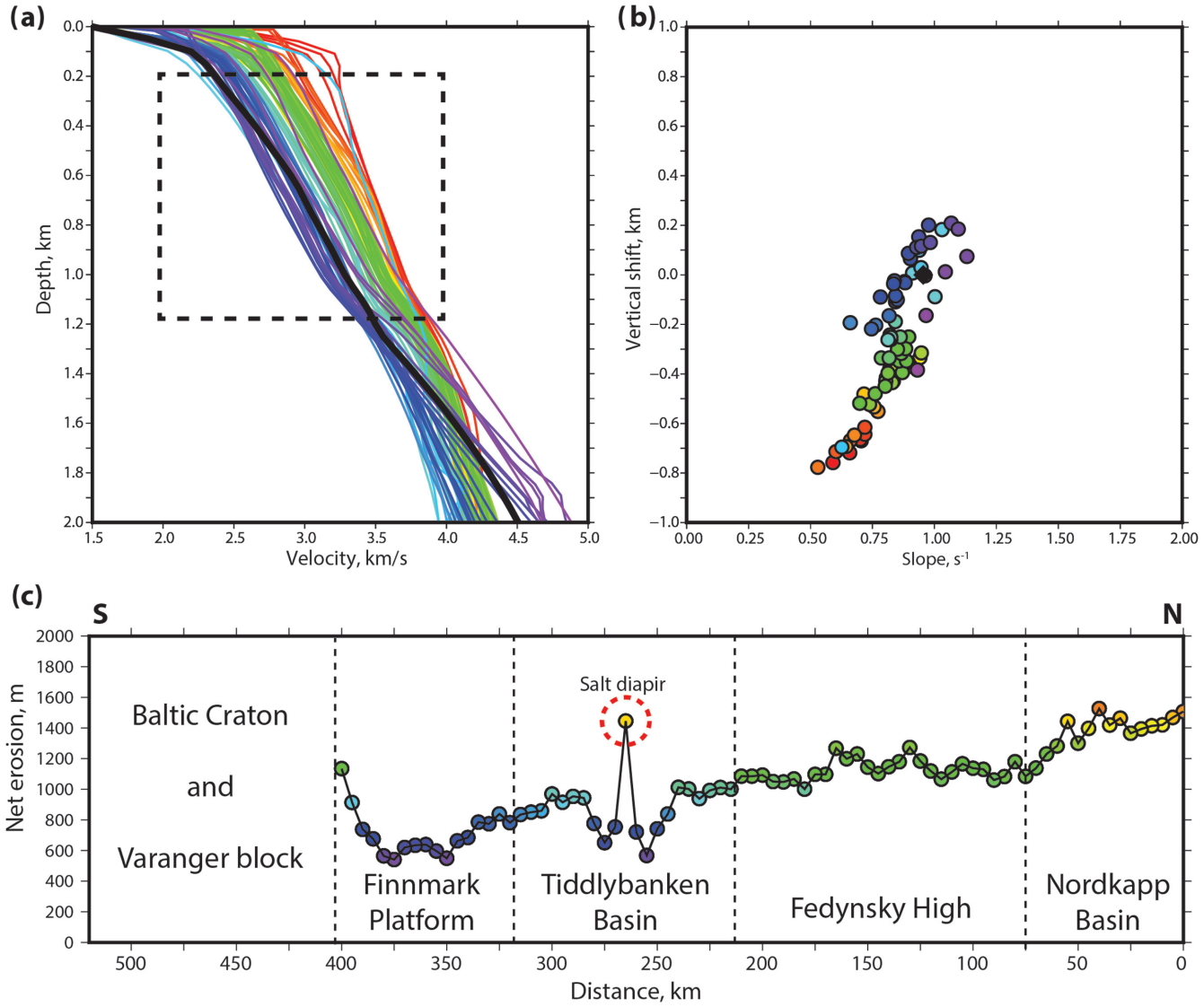

Figure 8. Estimation of the net erosion from the velocity profiles in the sediments. (a) The velocity profiles extracted every 1 km from the tomography model (zero depth corresponds to the sea floor). Colour-coding corresponds to sequential profile position in the rainbow pattern: red—north; blue—south; green—middle. The black line shows the reference velocity profile (from the Ludlovskaya borehole site; Gramberg *et al.* 1985); dashed box—gradient analysis window. (b) Individual velocity profiles plotted in depth-slope domain with respect to reference site (black diamond in the centre). (c) Along profile plot of the estimated uplift rates, assuming 750 m uplift on the Ludlovskaya reference site. The outlier at *ca.* 260 km distance represents a salt diapir in Tiddlybanken Basin.

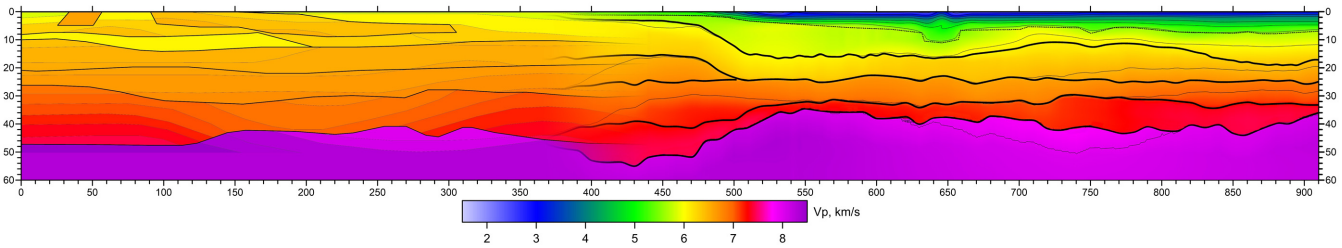

Figure 9. A combined plot, showing results from two different seismic profiles merged together (see Fig. 1 for locations). The colour-coding is identical for both profiles and represents Vp velocities. Left—results of the EGT Polar profile (Luosto *et al.* 1989); right—results from the present study. The overlap zone of two profiles is located between offsets 380–470 km.

crust appears to be semi-constant throughout the profile, the Moho depth increase is due to thickening of the lower and lowermost crust.

6.2 Nature of the high-velocity lower crustal bodies

The results of the seismic and gravity models resolve two areas along the profile with very high-velocity and -density LCBs. From

the resolution analysis the very high velocities in both zones are well constrained by the data. One is located below the Varanger Peninsula and the other one is observed below the Fedynsky High and surrounding areas. The presence of the LCBs at the other parts of the profile is questionable. If LCBs are present in other areas, their thickness does not exceed 1–1.5 km.

The LCB below the Varanger Peninsula represents a 70–100 km wide layer. Geometrically the layer is observed with a lens-like form, with a maximum thickness of about 15 km. The southern limit of the layer is located approximately below the shoreline near Kirkenes, which is about 50 km south of the Trollfjorden-Komagelva Fault Zone. The northern limit is located below the bathymetric depression north of the Varanger Peninsula, on the continuation of the ridge structure to the southeast (Fig. 2; approximately OBS-4).

The presence of high-velocity middle and lower crust and LCB can be linked with the numerous mafic dykes observed on the Varanger Peninsula. These document volcanic episodes in the area, which probably have been affecting the crustal structure by emplacement of intrusive bodies within the crustal volume as a mafic underplated layer at the base of the crust (Thybo & Artemieva 2013). Such a mechanism explains the observed high crustal velocities and densities. As the model is unable to provide independent constraint on the age of the magmatism, we consider several scenarios. The crustal emplacement of the mafic material together with the underplating can be of the Ediacaran (560–550 Ma) age, corresponding to the Timan orogenesis, and thus be a direct analogue to the structures observed further southeast around Timan Ridge and Pechora Basin (Kostyuchenko *et al.* 2006, Lorenz *et al.* 2013). Alternatively, some of the dykes on the Varanger Peninsula have been dated to Middle-Late Devonian (Guise & Roberts 2002). These ages are close to the end of the culmination of the Caledonian event, and the magmatism is likely post-dating the main Caledonian deformation and not directly related to it. The origin of the magmatic activity is unknown, but it might be linked with kimberlitic magmatism of the Kola Alkaline province (Mahotkin *et al.* 2000). This may indicate a mantle thermal anomaly below the White Sea during the Late Devonian with effect on the areas in the southern Barents Sea in terms of localized magmatism along pre-existing weak zones. Furthermore, the magmatic anomaly may also be connected with Devonian mafic magmatism observed in the northern East European Craton (Wilson *et al.* 1999; Pease *et al.* 2016). A linear chain of Devonian basaltic bodies is observed between the Varanger Peninsula and the Kanin Peninsula into the Timan range. In this scenario, the emplacement of the mafic melts at the base of the crust can be attributed to local melting of transitional mantle and lower crust during rifting of the continental domain (Pease *et al.* 2016). The tectonic movement of the Varanger block activated the bounding faults, which may have increased the potential for intrusive material to intrude into the crust from the LCB and localize the volcanic bodies around the Trollfjorden-Komagelva Fault.

The other well-resolved LCB below the Fedynsky High is observed from the northern part of the Tiddlybanken Basin and reaches its maximum thickness of 10 km beneath the Fedynsky High. The formation time of this LCB is unclear, but it may be connected with a thin high velocity sill structure in the pre-Carboniferous sedimentary strata. The high-velocity layer is not well resolved, but the Vp is estimated to be around 6.2–6.3 km s^{-1}. Based on these velocities this layer may be a mafic sill (Aarseth *et al.* 2017). If the sill and LCB are linked, they would have formed in the Devonian or earlier. A clue on its origin can be provided from the regional magnetic data (Fig. 10). The positive magnetic anomaly around Fedynsky High can be linked with the onshore Pechora Fault zone in the NW-SE trend. The SE Barents Basin located on this trend likely hides the magnetic signal due to extreme thickness of the sedimentary cover. Such interpretation suggests the age of the magmatism to be early Palaeozoic, which make a direct link of the modelled LCB to the ones reported under the onshore Pechora Basin (Kostyuchenko *et al.* 2006).

6.3 Crustal thinning by extension

We observe clear evidence for crustal extension and thinning in four regions along the profile. The estimated maximum extension ranges from 1.4 to 2 (Fig. 7). The Nordkapp Basin close to the northern edge of the profile is a rift structure formed in the Carboniferous (Faleide *et al.* 2008). Our profile samples this basin close to its NE termination where it is not fully manifested. Comparison of the crustal structure with the adjacent part further south along the profile shows 5–7 km thinning of the upper crust, while the lower crust is semi-constant along the profile.

The Tiddlybanken Basin is another example of a rift structure. The graben in the central part of the basin was formed by Carboniferous rifting, followed by later subsidence of rim-synclines of the salt diapirs in the middle-late Triassic and reactivation of salt movements after early Cretaceous. However, it is likely that the graben formed along pre-existing weak zones that came into existence either during Edicaran formation of the Timanides or during the Devonian rifting of the East European Craton, possibly simultaneously with the formation of the Nordkapp Basin. The structure of the crystalline crust does not show any significant thinning compared to the Finnmark Platform, but the upper crust is 3–5 km thinner than on the Fedynsky High, which shows the smallest extension.

The Finnmark Platform, bounded by the Tiddlybanken Basin and the Varanger block, shows the largest sedimentary thickness along the profile. We estimate the depth to the top basement to be *ca.* 15 km below the platform. In addition, the upper crust shows the lowest velocities along the profile: 6.2 km s^{-1}. Most likely the low velocities in the upper crust are caused by extensional faulting, occurring simultaneously with sediment accumulation and basin subsidence. The presence of the Varanger block further south, with its own lateral and vertical motions, complicates the estimation of the timing of platform extension, but most likely it is contemporaneous or slightly earlier than the formation of the Tiddlybanken Basin.

6.4 Evolution of the Fedynsky High

One on the most significant features along the profile is the Fedynsky High. Its expression is mainly by elevated basement, as the current bathymetry is strongly modified by glacial erosion. The long wavelength of the uplift favours a deep originating process, presumably in the upper mantle. There may be a link with the presence of the LCB, to similar structures below Pechora Basin, formed during Palaeozoic rifting. This suggests that the Fedynsky High is a long-existing feature on the present Barents shelf. It is likely that the basement high together with the underlying LCB formed around fault zones that were active in the Devonian or earlier. The formation of the Carboniferous rift through the Fedynsky High may provide indirect confirmation of this interpretation. This rift structure is clearly observed in the reflection line (Fig. 4), and it is likely that it developed at pre-existing weakness zones where faults were reactivated. The short wavelength perturbations of the basement are

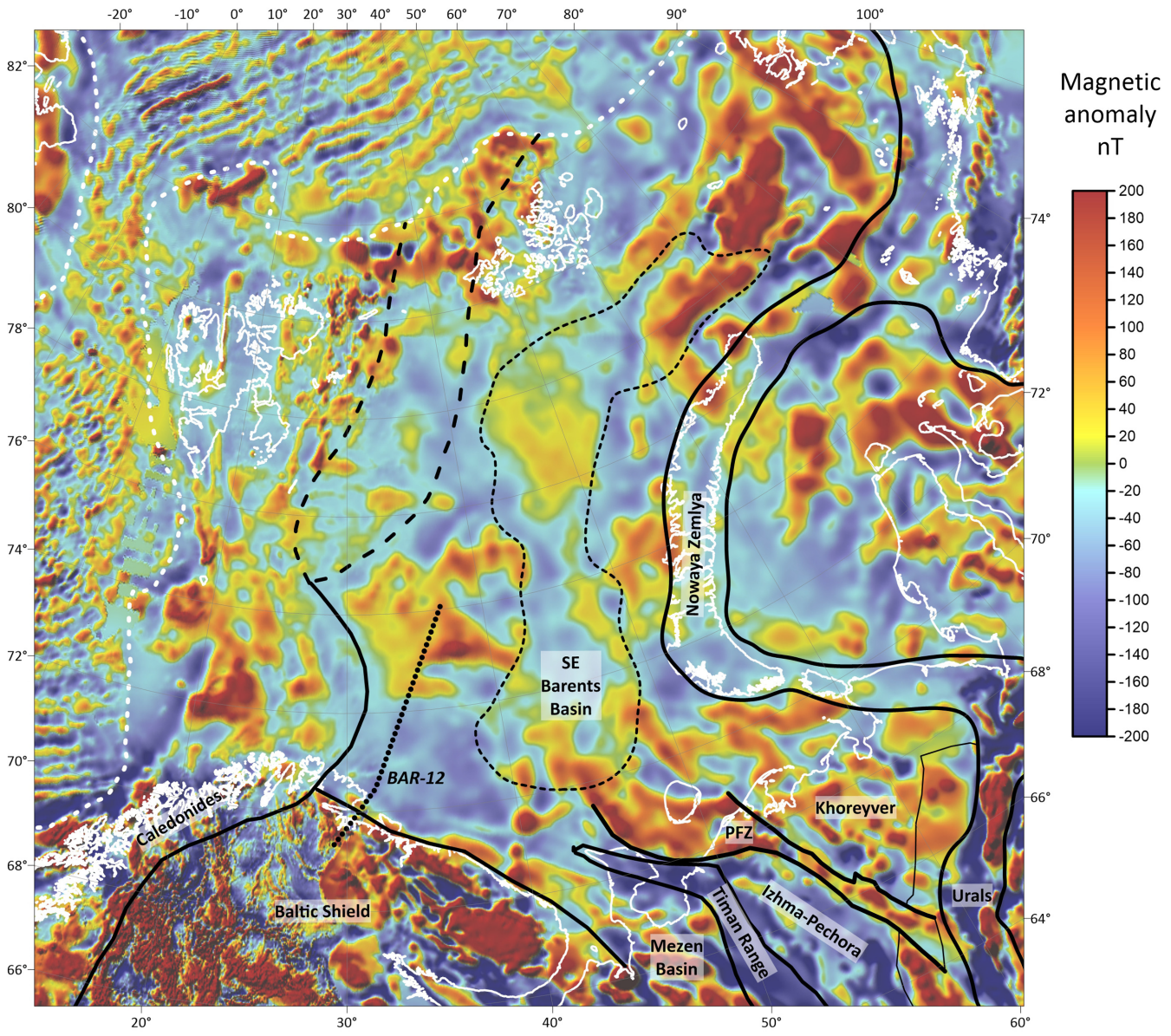

Figure 10. Magnetic anomaly map of the Greater Barents Sea, based on the CAMP-GM database (Gaina *et al.* 2011). Continent-ocean transition is marked by white stippled line. Major terrain boundaries are shown in black. PFZ—pre-Pechora Fault Zone. The location of the profile is also marked.

likely younger. They probably formed in the compression regime during the final closure of the Uralian Ocean and upthrusting of Novaya Zemlya in the Late Triassic, which likely extended into the early Jurassic (Faleide *et al.* 2018), and with a main contraction phase later than Early Cretaceous. Therefore, both vertical forces originating from the mantle and horizontal tectonic stresses may have controlled the evolution of the Fedynsky High.

7 CONCLUSIONS

We present the first complete crustal-scale model of the former disputed zone between Norway and Russia based on a seismic refraction/wide-angle reflection profile (Fig. 11). The model provides basis for improving our understanding of the evolution of the Greater Barents Sea region, as it covers the transition between the western and eastern domains that have different structure and tectonic evolution.

Our model documents the transition from the Baltic craton to the Barents shelf. The deep crustal structure below the Varanger Peninsula, at the northern edge of the craton, suggests that it is an independent crustal block, which was heavily modified either by Edicaran or by Devonian magmatism. Its crustal thickness is estimated to reach 47–51 km, with high velocities in the middle and lower crust. A very high-velocity and -density LCB is observed below the Varanger Peninsula with a maximum thickness of 11 km.

Large volumes of pre-Carboniferous sedimentary strata are documented in the offshore part of the profile with thicknesses that exceed 10 km, in particular on the Finnmark Platform. Here, this unit may consist of both Devonian molasses and underlying early Palaeozoic meta-sediments.

The elevated basement in the Fedynsky High laterally coincides with the location of a large very high-velocity LCB at the base of the crust with a thickness of up to 10 km. We interpret the high

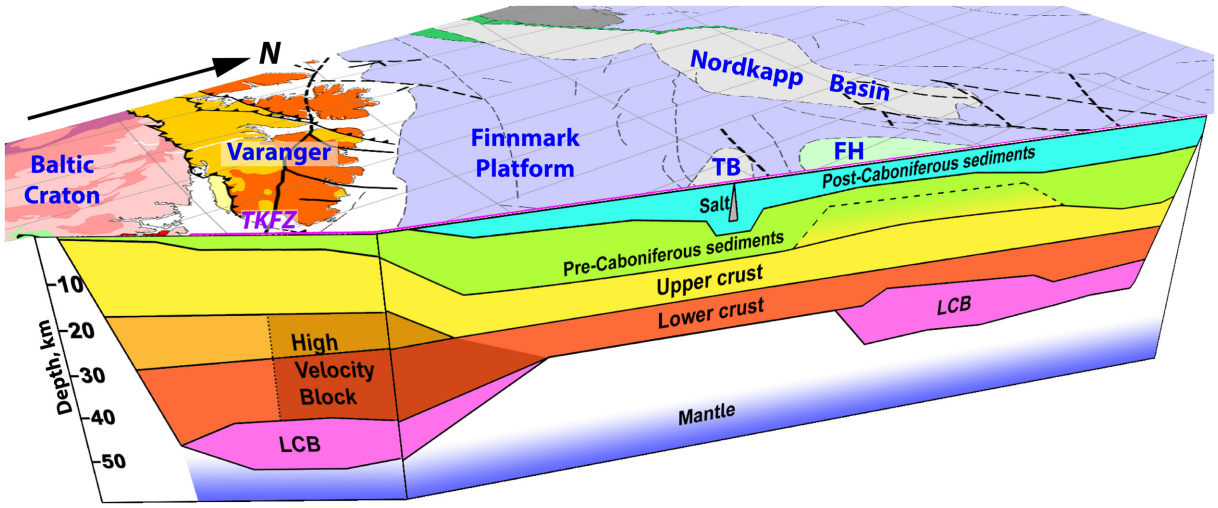

Figure 11. A 3-D sketch of the crustal structure in the profile based on joint interpretation of the seismic and gravity models. The major features observed are the distinct change in the properties across the Trollfjorden-Komagelva Fault Zone (TKFZ) and the presence of large volumes of lower crustal bodies (LCB) beneath the Varanger Peninsula and Fedynsky High. TB—Tiddlybanken Basin; FH—Fedynsky High.

as being a long-existing feature that formed before or during the Devonian in association with extensive magmatic activity.

We propose that the LCBs below the Varanger Peninsula and the Fedynsky High are inherited features from the Timanides similar to mafic structures on the Kanin Peninsula, Timan Ridge, and Pechora Basin or formed later during the Devonian extension, associated with the continental rifting in the northern East European Craton. The formation of the Tiddlybanken Basin and may be the Finnmark Platform could also be connected to the rifting processes in the East European Craton in the Devonian. A large part of the present sedimentary cover may have accumulated in basement lows formed during this rifting episode.

ACKNOWLEDGEMENTS

The Norwegian Petroleum Directorate is thanked for funding the survey and data analysis, for providing interpreted MCS data and for giving permission to publish this paper. We thank in particular Dag Bering and Harald Brekke. We acknowledge the Research Council of Norway through its Centres of Excellence funding scheme, project number 223272. We would like to thank two anonymous reviewers, their comments significantly helped to improve the manuscript. We thank the OBS and land teams: Audun Libak, Helge Johnsen, Espen Lehn-Nilsen, Alexander Minakov, Anke Dannowski, Wiebke Leuchters, Martin Thorwart, Thorge Wiskandt and Helene Kraft. We would like to thank the captain of R/V 'Håkon Mosby' and his crew for their enormous help and support during the cruise.

REFERENCES

Aarseth, I. *et al.*, 2017. Crustal structure and evolution of the Arctic Caledonides: results from controlled-source seismology, *Tectonophysics,* **718,** 9–24.

Anell, I., Thybo, H. & Artemieva, I.M., 2009. Cenozoic uplift and subsidence in the North Atlantic region: geological evidence revisited, *Tectonophysics,* **474,** 78–105.

Artemieva, I.M., Thybo, H. & Kaban, M.K., 2006. Deep Europe today: geophysical synthesis of the upper mantle structure and lithospheric processes over 3.5 Ga, in *European Lithosphere Dynamics,* Vol. **32,** pp. 11–41, eds Gee, D.G. & Stephenson, R.A., Geological Society, London, Memoirs.

Baig, I., Faleide, J.I., Jahren, J. & Mondol, N.H., 2016, Cenozoic exhumation on the southwestern Barents shelf: estimates and uncertainties constrained from compaction and thermal maturity analyses, *Mar. Pet. Geol.,* **73,** 105–130.

Barrere, C., Ebbing, J. & Gernigon, L., 2011. 3-D density and magnetic crustal characterisation of the southwestern Barents shelf: implications for the offshore prolongation of the Norwegian Caledonides, *Geophys. J. Int.,* **184,** 1147–1166.

Bialas, J. & Flueh, E.R., 1999. Ocean bottom seismometers, *Sea Technol.,* **40**(4), 41–46.

Breivik, A.J., Mjelde, R., Grogan, P., Shimamura, H., Murai, Y. & Nishimura, Y., 2003. Crustal structure and transform margin development south of Svalbard based on ocean bottom seismometer data, *Tectonophysics,* **369,** 37–70.

Breivik, A.J., Mjelde, R., Grogan, P., Shimamura, H., Murai, Y. & Nishimura, Y., 2005. Caledonide development offshore–onshore Svalbard based on ocean bottom seismometer, conventional seismic and potential field data, *Tectonophysics,* **401,** 79–117.

Carlson, R.L. & Herrick, C.N., 1990. Densities and porosities in the oceanic crust and their variations with depth and age, *J. geophys. Res.,* **95,** 9153–9170.

Christensen, N.I. & Mooney, W.D., 1995. Seismic velocity structure and composition of the continental crust: a global view, *J. geophys. Res.,* **100,** 9761–9788.

Churkin, M.J., Soleimani, G., Carter, C. & Robinson, R., 1981. Geology of the Soviet Arctic: Kola Peninsula to Lena river, in *The Ocean Basins and Margins, The Arctic Ocean,* Vol. **5,** pp. 331–375, eds Nairn, A.E.M., Churkin, M.J. & Stehli, F.G., Plenum Press.

Clark, S.A., Faleide, I.J., Hauser, J., Ritzmann, O., Mjelde, R., Ebbing, J., Thybo, H. & Flueh, E., 2013. Stochastic velocity inversion of seismic reflection/refraction traveltime data for rift structure of the southwest Barents Sea, *Tectonophysics,* **593,** 135–150

Corfu, F., Polteau, S., Planke, S., Faleide, J., Svensen, H., Zayonchek, A. & Stolbov, N., 2013. U–Pb geochronology of Cretaceous magmatism on Svalbard and Franz Josef Land, Barents Sea Large Igneous Province, *Geol. Mag.,* **150**(6), 1127–1135.

Faleide, J.I., Vågnes, E. & Gudlaugsson, S.T., 1993, Late Mesozoic-Cenozoic evolution of the southwestern Barents Sea in a regional riftshear tectonic setting, *Mar. Pet. Geol.,* **10,** 186–214.

Faleide, J.I., Tsikalas, F., Breivik, A.J., Mjelde, R., Ritzmann, O., Engen, O., Wilson, J. & Eldholm, O., 2008. Structure and evolution of the continental margin off Norway and Barents Sea, *Episodes,* **31**(1), 82–91.

Faleide, J.I., Pease, V., Curtis, M., Klitzke, P., Minakov, A., Scheck-Wenderoth, M., Kostyuchenko, S. & Zayonchek, A., 2018. Tectonic implications of the lithosphere structure across the Barents and Kara shelves, *Circum-Arctic Lithopheric Evolution,* Pease, V. & Coakley, B., **460,** Geological Society, London Special Publications.

Gabrielsen, R.H., Færseth, R.B., Jensen, L.N., Kalheim, J.E. & Riis, F., 1990. Structural elements of the Norwegian continental shelf. Part1: the Barents Sea Region, *Norwegian Pet. Direct. Bull.,* **6,** 1–47.

Gac, S., Klitzke, P., Minakov, A., Faleide, J.I. & Scheck-Wenderoth, M., 2016. Lithospheric strength and elastic thickness of the Barents Sea and Kara Sea region, *Tectonophysics,* **691,** 120–132.

Gaina, C., Werner, S., Saltus, R. & Maus, S., & the CAMP-GM group. 2011. Circum-Arctic mapping project: new magnetic and gravity anomaly maps of Arctic, in *Arctic Petroleum Geology,* pp 39–48, eds Spencer, A.M., Embry, A.F., Gautier, D.L., Stoupakova, A.V. & Sørensen, K., Geological Society, London, Memoirs.

Gee, D.G., Bogolepova, O.K. & Lorenz, H., 2006. The Timanide, Caledonide and Uralide orogens in the Eurasian high Arctic, and relationships to the palaeo-continents Laurentia, Baltica and Siberia, in *European Lithosphere Dynamics,* Vol. **32,** pp. 507–520, eds Gee, D.G. & Stephenson, R.A., Geological Society, London, Memoirs.

Gee, D.G., Fossen, H., Henriksen, N. & Higgins, A.K., 2008. From the early Paleozoic platforms of Baltica and Laurentia to the Caledonide Orogen of Scandinavia and Greenland, *Episodes,* **31**(1), 44–51.

Gernigon, L. & Bronner, M., 2012. Late Palaeozoic architecture and evolution of the southwestern Barents Sea: insights from a new generation of aeromagnetic data, *J. Geol. Soc.,* **169,** 449–459.

Gernigon, L., Brönner, M., Roberts, D., Olesen, O., Nasuti, A. & Yamasaki., T., 2014. Crustal and basin evolution of the southwestern Barents Sea: from Caledonian orogeny to continental breakup, *Tectonics,* **33,** 347–373.

Gramberg, I.S., Shkola, I.V., Bro, Y.G., Shekhodanov, V.A. & Armishev, A.M., 1985. Parametric wells on the islands in the Barents and Kara seas, *Sovetskaya Geol.,* **1,** 95–98.

Grogan, P., Nyberg, K., Fotland, B., Mykelbust, R., Dahlgren, S. & Riis, F., 1998. Cretaceous magmatism south and east of Svalbard: evidence from seismic reflection and magmatic data, *Polarforschung,* **68,** 25–34.

Gudlaugsson, S.T., Faleide, J.I., Johansen, S.E. & Breivik, A.J., 1998. Late Palaeozoic structural development of the Southwestern Barents Sea, *Mar. Pet. Geol.,* **15**(1), 73–102.

Guise, P.G. & Roberts, D., 2002. Devonian ages from 40Ar/39Ar dating of plagioclase in dolerite dykes, eastern Varanger Peninsula, North Norway, *Norges geologiske undersokelse,* **440,** 27–37.

Hauser, J., Dyer, K.M., Pasyanos, M.E., Bungum, H., Faleide, J.I., Clark, S.A. & Schweitzer, J., 2011. A probabilistic seismic model for the European Arctic, *J. geophys. Res.,* **116,** 1–17.

Henriksen, E., Ryseth, A.E., Larssen, B.G., Heide, T., Rønning, K. & Stoupakova, A.V., 2011a. Tectonostratigraphy of the greater Barents Sea: implication for petroleum systems, in *Arctic Petroleum Geology,*Vol. **35,** eds Spencer, A.M., Embry, A.F., Gautier, D.L., Stoupakova, A. & Sørensen, K., Geological Society, London, Memoirs.

Henriksen, E. *et al.*, 2011b. Uplift and erosion of the greater Barents Sea: impact on prospectivity and petroleum systems, in *Arctic Petroleum Geology,* eds Spencer, A.M., Embry, A.F., Gautier, D.L., Stoupakova, A. & Sørensen, K., Geological Society, London, Memoirs.

Herrevold, T., Gabrielsen, R.H. & Roberts, D., 2009. Structural geology of the southeastern part of the Trollfjorden-Komagelva Fault Zone, Varanger Peninsula, Finnmark, North Norway, *Norw. J. Geol.,* **89,** 305–325.

Ivanova, N.M., Sakulina, T.S., Belyaev, I.V., Matveev, Y.I. & Roslov, Y.V., 2011. Depth model of the Barents and Kara seas according to geophysical surveys results, in *Arctic Petroleum Geology,* Vol. **35,** pp. 209–221, eds Spencer, A.M., Embry, A.F., Gautier, D.L., Stoupakova, A. & Sørensen, K., Geological Society, London, Memoirs.

Johansen, S.E., Henningsen, T., Rundhovde, E., Saether, B.M., Fichler, C. & Rueslatten, H.G., 1994. Continuation of the Caledonides North of Norway—seismic reflectors within the basement beneath the Southern Barents Sea, *Mar. Pet. Geol.,* **11**(2), 190–201.

Klitzke, P., Faleide, J.I., Schcke-Wenderoth, M. & Sippel, J., 2015. A lithosphere-scale structural model of the Barents Sea and Kara Sea region, *Solid Earth,* **6,** 153–172.

Korenaga, J., Holbrook, S., Kent, G., Kelemen, P., Detrick, R.S., Larsen, H.-C., Hopper, J.R. & Dahl-Jensen, T., 2000. Crustal structure of the southeast Greenland margin from joint refraction and reflection seismic tomography, *J. geophys. Res.,* **105,** 21 591–21 614.

Kostyuchenko, S., Sapozhnikov, R., Egorkin, A., Gee, D., Berzin, R. & Solodilov, L., 2006. Crustal structure and tectonic model of northeastern Baltica, based on deep seismic and potential field data, in *European Lithosphere Dynamics,* Vol. **32,** pp. 521–539, eds Gee, D.G. & Stephenson, R.A., Geological Society, London, Memoirs.

Luosto, U. *et al.*, 1989. The crustal structure along the polar profile from seismic refraction investigations, *Tectonophysics,* **162**(1-2), 51–85.

Maher, H.D., 2001. Manifestations of the Cretaceous High Arctic Large Igneous Province in Svalbard, *J. Geol.,* **109**(1), 91–104.

Mahotkin, I.L., Gibson, S.A., Thompson, R.N., Zhuravlev, D.Z. & Zherdev, P.U., 2000. Late devonian diamondiferous kimberlite and alkaline picrite (Proto-Kimberlite?) magmatism in the arkhangelsk region, NW Russia, *J. Petrol.,* **41**(2), 201–227.

Marello, L., Ebbing, J. & Gernigon, L., 2013. Basement inhomogeneities and crustal setting in the Barents Sea from a combined 3-D gravity and magnetic model, *Geophys. J. Int.,* **193,** 557–584.

Medvedev, S. & Hartz, E.H., 2015, Evolution of topography of post-Devonian Scandinavia: effects and rates of erosion, *Geomorphology,* **231,** 229–245.

Minakov, A., Mjelde, R., Faleide, J.I., Flueh, E., Dannowski, A. & Keers, H., 2012a. Mafic intrusions east of Svalbard imaged by active source seismic tomography, *Tectonophysics,* **518,** 106–118.

Minakov, A., Faleide, J.I., Glebovsky, V.Y. & Mjelde, R., 2012b. The structure and evolution of the Northern Barents–Kara Sea continental margin from integrated analysis of potential field, bathymetry and sparse seismic data, *Geophys. J. Int.,* **188,** 79–102.

Minakov, A., Yarushina, V., Faleide, J.I., Krupnova, N., Sakoulina, T., Dergunov, N. & Glebovsky, V., 2017. Dyke emplacement and crustal structure within a continental large igneous province, northern Barents Sea, Geological Society, London, Special Publications, doi:10.1144/SP460.4.

Lorenz, H., Gee, D.G., Korago, E., Kovaleva, G., McClelland, W.C., Gilotti, J.A. & Frei, D., 2013. Detrital zircon geochronology of Palaeozoic Novaya Zemlya—a key to understanding the basement of the Barents Shelf, *TerraNova,* **25,** 496–503.

Olovyanishnikov, V., Roberts, D. & Siedlecka, A., 2000. Tetonics and sedimentation of the Meso- to Neoproterozoic Timan-Varanger Belt along the Northeastern Margin of Baltica, *Polarforschung,* **68,** 267–274.

Otto, S.C. & Bailey, R.J., 1995. Tectonic evolution of the Northern Ural Orogen, *J. Geol. Soc.,* **152,** 903–906.

Pease, V., 2011. Eurasian orogens and Arctic Tectonics: an overview, in *Arctic Petroleum Geology,* Vol. **35,** pp. 311–324, eds Spencer, A.M., Embry, A.F., Gautier, D.L., Stoupakova, A.V. & Sørensen, K., Geological Society, London, Memoirs.

Pease, V. & Scott, R.A., 2009. Crustal affinities in the Arctic Uralides, northern Russia: significance of detrital zircon ages from Neoproterozoic and Palaeozoic sediments in Novaya Zemlya and Yaimir, *J. Geol. Soc.,* **166,** 517–527.

Pease, V., Scarrow, J.H, Nobre Silva, I.G. & Cambeses, A., 2016. Devonian magmatism in the Timan Range, Arctic Russia - subduction, post orogenic extension, or rifting?, *Tectonophysics,* **691**(8), 185–197.

Polteau, S. *et al.*, 2016. The early cretaceous barents sea sill complex: distribution, Ar/Ar geochronology and implications for carbon gas formation, *Palaeogeogr. Palaeoclimatol. Palaeoecol.,* **441,** 83–95.

Puchkov, V., 2002. Paleozoic evolution of the east European continental margin involved in the Uralide Orogeny, in *Mountain Building in the Uralides: Pangea to the Present,* pp. 9–31, eds Brown, D., Juhlin, C. & Puchkov, V., American Geophysical Union.

Ritzmann, O. & Faleide, J.I., 2007. Caledonian basement of the western Barents Sea, *Tectonics,* **26**(5), doi:10.1029/2006TC002059.

Ritzmann, O. & Faleide, J.I., 2009. The crust and mantle lithoshere in the Barents Sea/Kara Sea region, *Tectonophysics,* **593,** 135–150.
Ritzmann, O., Maercklin, N., Faleide, J.I., Bungum, H., Mooney, W.D. & Detweiler, S.T., 2007. A three-dimensional geophysical model of the crust in the Barents Sea region: model construction and basement characterization, *Geophys. J. Int.,* **170,** 417–435.
Roberts, D., 2003. The Scandinavian Caledonides; event chronology, palaeogeographic settings and likely modern analogues, *Tectonophysics,* **365,** 283–299.
Roberts, D. & Siedlecka, A., 2002. Timanian orogenic deformation along the northeastern margin of Baltica, Northwest Russia and Northeast Norway, and Avalonian–Cadomian connections, *Tectonophysics,* **352,** 169–184.
Roberts, D., Chand, S. & Rise, L., 2011. A half-graben of inferred Late Palaeozoic age in outer Varangerfjorden, Finnmark: evidence from seismic-reflection profiles and multibeam bathymetry, *Norw. J. Geol.,* **91,** 191–200.
Roslov, Yu.V., Sakoulina, T.S. & Pavlenkova, N.I., 2009. Deep seismic investigations in the Barents and Kara Seas, *Tectonophysics,* **472,** 301–308.
Sakoulina, T.S., Telegin, A.N., Tikhonova, I.M., Verba, M.L., Marveev, Y.I., Vinnick, A.A., Kopylova, A.V. & Dvornikov, L.G., 2000. The results of deep seismic investigations on geotraverse in the Barents Sea from Kola Peninsula to Franz-Joseph Land, *Tectonophysics,* **329,** 319–331.
Talwani, M., Krishna, K.S., Ismaiel, M. & Desa, M.A., 2017. Comment on a paper by Sibuet *et al.* (2016) entitled "Thinned continental crust intruded by volcanics beneath the northern Bay of Bengal", *Mar. Pet. Geol.,* **88,** 1123–1125.
Thybo, H. & Artemieva, I.M., 2013. Moho and magmatic underplating in continental lithosphere, *Tectonophysics,* **609,** 605–619.
Wilson, M., Wijbrans, J., Fokin, P.A., Nikishin, A.M., Gorbachev, V.I. & .Nazarevich, B.P, 1999. $^{40}Ar/^{39}Ar$ dating, geochemistry and tectonic setting of Early Carboniferous dolerite sills in the Pechora basin, foreland of the Polar Urals, *Tectonophysics,* **313**(8), 107–118.
Zelt, C.A. & Smith, R.B., 1992. Seismic traveltime inversion for 2-D crustal velocity structure, *Geophys. J. Int.,* **108,** 16–34.

SUPPORTING INFORMATION

Supplementary data are available at *GJI* online.
Figure S1. Simplified modelling flow chart showing the major steps. Green fields (OBS and MCS data)—input data; red fields—data processing steps; blue and violet boxes—modelling steps. Detailed description is provided in the main text.
Please note: Oxford University Press is not responsible for the content or functionality of any supporting materials supplied by the authors. Any queries (other than missing material) should be directed to the corresponding author for the paper.